



Using Physical and Soft Computing Models to Evaluate Discharge Coefficient for Combined Weir–Gate Structures Under Free Flow Conditions

Behnam Balouchi¹ · Gholamreza Rakhshandehroo¹

Received: 30 November 2016 / Accepted: 15 May 2018 / Published online: 22 May 2018
© Shiraz University 2018

Abstract

In this study, a single triangular sharp-crested weir and four combined structures consisting of the weir and rectangular gates with different dimensions were tested to find the effects of water head over the weir (h) and geometric parameters such as gate height (d), gate breadth (b), and the distance between top of the gate and bottom of the weir (y) on discharge coefficient (C_d) under free flow conditions. A new form was proposed for the equation used to compute C_d , which is based on a combination of triangular weir and rectangular gate equations. Experimental results showed that as dimensionless ratios of h/d , h/b , and h/y increased, the discharge coefficient and total discharge increased, too. Additionally, discharge coefficient for the combined weir–gate increased with increasing gate opening at same flow rates. It was concluded that, at low discharges, the gate and its opening are the main water head controllers, while water levels at high discharges are mainly controlled by the weir. The two utilized soft computing models (MLP and SVR) predicted C_d accurately, with R^2 values (for total data) of 0.966 and 0.967, respectively. However, MLP was considered superior, due to its better statistical indices of RMSE, MAE, and R^2 (0.027, 0.022, and 0.984, respectively) for validation data set compared to those of SVR (0.065, 0.042, and 0.948, respectively). Comparison of results with equations presented in the literature showed that some equations match the observed data much better than others, which are noticeably different. It was concluded that assuming the general form of a gate or a triangular weir equation for a combined weir–gate structure shall be reconsidered before its utilization in particular applications.

Keywords Discharge coefficients · Free flow · Combined structure · Triangular weir · Rectangular gate · MLP · SVR

List of Symbols

A_g	Gate area	h	Water head over the weir
b	Gate width	H	Upstream water depth
b_1	Weir breadth	h_d	Depth of water just downstream the gate
B	Channel width	k	Kernel function in SVR
C	Regularization cost parameter in SVR	N	Number of data set in RMSE and MAE equation
C_d	Discharge coefficient	Q_t	Total combined structure discharge
d	Gate height	Re	Reynolds numbers
Fr	Froude numbers	v	Fluid velocity
g	Gravity acceleration	w_{ij}	Weight of the connection between the j th neuron in a layer with the i th neuron in the previous layer of ANN
		We	Weber numbers
		x_i	Value of the i th neuron in the previous layer of ANN
		y	Distance between top of the gate and bottom of the weir
		Y_i	Prediction parameter in RMSE and MAE equation (C_d in this study)
		y_j	Output from the j th neuron in a given layer of ANN

✉ Behnam Balouchi
behnam_1988@yahoo.com
Gholamreza Rakhshandehroo
rakhshan@shirazu.ac.ir

¹ Department of Civil and Environmental Engineering, Shiraz University, Shiraz, Iran

ε	Size of error insensitive zone in SVR
θ	Top angle of the triangular weir
σ	Surface tension
ρ	Flow density
μ	Fluid dynamic viscosity
γ	Kernel specific parameter in SVR

1 Introduction

Weirs and gates are common and important structures usually used to control and measure flow in open channels. In waterways with alluvial beds where weirs are used, sediments deposit upstream of the weir, reduce its effective height over time, and ultimately deteriorate its performance. Compared to a single weir, a combined weir–gate structure may be used to measure flow discharge and, at the same time, avoid sediment deposition behind the structure.

As classical flow measuring devices, researchers have carried out extensive studies on flow over triangular sharp-crested weirs and through rectangular gates. Rajaratnam (1977), French (1986), Swamee (1992), Lozano et al. (2009), Habibzadeh et al. (2011), Belaud et al. (2012), and Khalili Shayan and Farhoudi (2013) were among researchers studying flow through gates (sluice gates). Among investigations conducted on weirs, studies by Swamee (1988), Bos (1989), Munson et al. (1994), Johnson (2000), Aydin et al. (2002), Martínez et al. (2005), Qu et al. (2009), Aydin et al. (2011), Chanson and Wang (2013), and Bautista-Capetillo et al. (2014) may be found in the literature.

Performance of a combined weir–gate structure has also been investigated by some researchers. Negm (1995) is among early researchers studying characteristics of a free combined flow over a rectangular weir with different side contractions and through a rectangular gate. El-Saiad et al. (1995) studied combined flow through high-discharge irrigation channels. They focused their investigations on a rectangular weir combined with a V-notch gate and a V-notch weir combined with a rectangular gate to present a flow estimation equation for both systems as:

$$\frac{Q_t}{\sqrt{2gd^{2.5}}} = -5.119 + 1.475 \left(\frac{H+h}{d} \right) - 2.531 \left(\frac{h}{b} \right) + 0.367 \left(\frac{b}{b_1} \right) + 1.2698 \quad (1)$$

They also concluded that the combination of a V-notch weir and a rectangular gate performs better than the combination of a rectangular weir and a V-notch gate.

Negm et al. (1997) studied the effect of downstream submergence on flow discharge and derived a set of

equations for free flow through a triangular weir over a contracting sluice gate and vice versa with specific restrictions. They concluded that the gate submergence ratio (tail water depth to the gate opening) affects upstream water height and flow discharge. They proposed the following equation for a triangular weir placed over a rectangular gate:

$$\frac{Q_t}{\sqrt{2gd^{2.5}}} = -0.019 + 0.875 \left(\frac{H+h}{d} \right) - 1.308 \left(\frac{h}{b} \right) + 0.005 \left(\frac{b}{b_1} \right) + 0.074\theta - 0.663 \left(\frac{h_d}{d} \right) \quad (2)$$

The following constraints were considered in derivation of Eq. 2:

$$1 < \frac{b}{d} < 3, 1 < \frac{y}{d} < 3, 2.9 < \frac{H+h}{d} < 7.9 \text{ and } 0.6 < \frac{b}{b_1} < 5.4.$$

Characteristics of combined flow through a triangular weir over a contracting rectangular gate were studied by Alhamid et al. (1997), too. He assumed that the combined weir–gate acts as a single gate and, therefore, derived a total discharge equation like that of a gate (a function of $H^1/2$):

$$Q_t = \left[0.84 + \frac{2.41 \tan\left(\frac{\theta}{2}\right)^{0.498} \left(\frac{h}{B}\right)^{1.56}}{\left(\frac{H}{y}\right)^{1.76} \left(\frac{d}{d+y}\right)^{0.325} \left(\frac{b}{B}\right)^{0.522}} \right]^4 \times A_g \sqrt{2gH} \quad (3)$$

The following constraints were considered in his study:

$$0.3 < \frac{y}{H} < 0.7, 0.17 < \frac{b}{B} < 0.5, 30 < \theta < 90, 0.35 < \frac{d}{d+y} < 0.5 \text{ and } H > (d+y).$$

Negm (2000) simulated a combined rectangular weir and a rectangular gate model and developed a relationship for the flow. He generalized his model and presented an equation for both free and submerged flows. Negm et al. (2002) conducted similar experiments on different channel slopes and analyzed their model with different geometries for both mild and steep slopes and presented an equation for all models. Hayawi et al. studied the effect of hydraulic and geometric parameters on the discharge coefficient computed from an equation similar to the rectangular weir equation. They present the following equation for prediction of total discharge:

$$\frac{Q_t}{g^{0.5}h^{2.5}} = 0.0197 \left(\frac{y}{h} \right)^{0.2195} \left(\frac{b}{h} \right)^{1.647} \left(\frac{d}{h} \right)^{0.543} \quad (4)$$

subject to the following constraints.

$$30 < \theta < 60, 0.05 < y < 0.15$$

Altan-Sakaraya and Kokpinar (2013) conducted experiments to find a discharge–depth relationship for



simultaneous flow through rectangular gates and over rectangular weirs.

In recent years, popularity of soft computing models has increased in various fields due to their capability for solving complex and nonlinear problems that might otherwise not have any tractable solution. Multilayer perceptron (MLP) artificial neural networks (ANN) and support vector machines (SVM) may be considered as two of the most popular soft computing models utilized in hydraulic applications. Baylar et al. (2009) used SVM to predict aeration performance of plunging overfall jets from weirs. Ozkan and Kaya (2010) used MLP and adaptive neuro-fuzzy inference system (ANFIS) models to predict air demand ratio in Venturi weirs. Bilhan et al. (2011) and Emiroghlu et al. (2011) used MLP, multiple linear and nonlinear regression models to predict discharge coefficient for a triangular labyrinth side weir in curved and straight channels, respectively. Juma et al. (2014) used MLP to determine discharge coefficient for a hollow semicircular crested weir. Mohammadpour et al. (2015) used SVM to predict water quality index in constructed wetlands. Balouchi et al. (2015) used ANN and M5P model tree to predict maximum scour depth at river confluences under live-bed conditions. Haghiabi et al. (2017) used MLP and SVM to predict head loss on a cascade weir. Their results show that SVM yields better results than MLP. Parsaie et al. (2017) evaluated ANFIS and MLP models for a cylindrical weir–gate similar to a broad crested weir and compared it with a sharp-crested weir. In their study, they showed that MLP is the superior model.

In the present study, four combined triangular weir and rectangular gate physical models with different gate dimensions, and a single weir physical model were constructed. Experiments were conducted for different discharges with extended measuring ranges for relevant parameters. Then, the effects of hydraulic and geometric parameters on discharge coefficient through these models were studied. MLP and support vector regression (SVR; as a certain type of SVM) models were constructed, trained, and tested to estimate discharge coefficients for a variety of combined weir–gate structures under different discharges. Results were compared with equations presented for flow through combined weir and gate structures in the literature.

2 Materials and Methods

Figure 1 shows the overall flowchart and methodology for this study. As shown, once dimensional analysis and experimental setup were completed, measurements were made and the effect of each non dimensional parameter on discharge coefficient was experimentally investigated. The collected data set was divided into training and validating

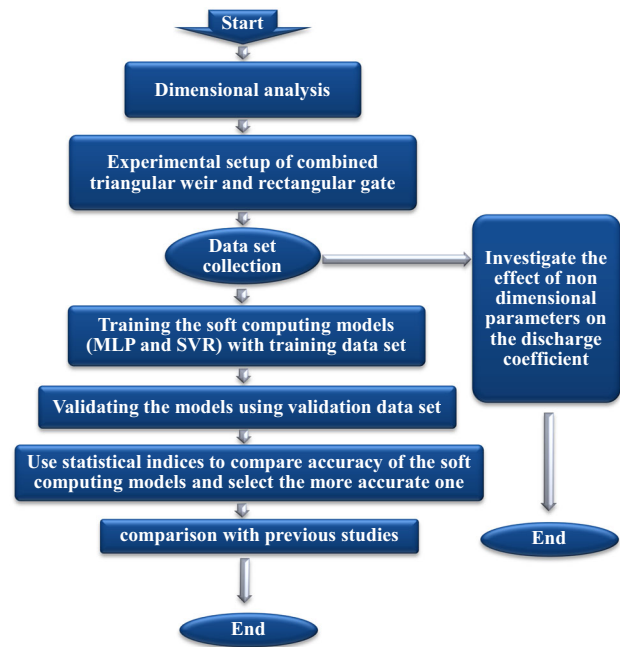


Fig. 1 Methodology flowchart for the current study

subsets and fed to the soft computing models. Statistical indices were used to compare accuracy of the models for discharge coefficient prediction in combined weir–gate structures. Finally, results were compared and contrasted with equations presented in previous studies for similar structures.

2.1 Physical Model Setup and Dimensional Analyses

A 11-m-long, 0.25-m-wide, and 0.5-m-deep rectangular channel in Hydraulic Laboratory of Water Engineering Department at Shahid Chamran University was used for experimental tests. Water was pumped into an elevated tank and fed into the channel with a constant rate, measured by a standard 53° triangular weir and a digital gage with 0.1 mm accuracy.

Four combined weir–gate structures and a single weir were all cut by a laser machine out of a 10-mm-thick Plexiglas sheet. All weirs were triangular ones with 60° top angles, and their top edges were beveled according to USBR standards. Figure 2 and Table 1 give variables and dimensions for the models. A total of 46 experiments were carried out with ranges of relevant dimensionless ratios as; $0.96 < \frac{h}{b} < 3.62$, $0.18 < \frac{h}{y} < 0.75$, $2.12 < \frac{h}{d} < 12.16$, $1 < \frac{b}{d} < 4$, $4.6 < \frac{y}{d} < 21.4$, $9.8 < \frac{(H+h)}{d} < 46.7$, and $0.045 < \frac{d}{(d+y)} < 0.18$.

Performing a dimensional analysis, similar hydraulic characteristics of utilized weirs and gates were combined.

Fig. 2 The physical model sketches and variables for combined weir–gate structures

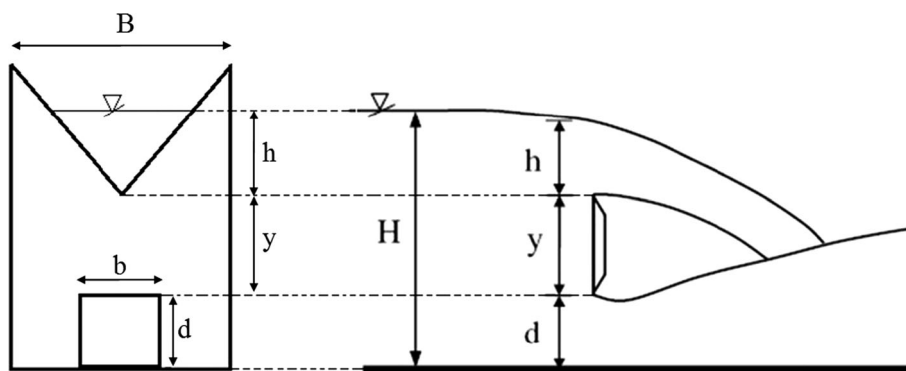


Table 1 Ranges of relevant variables for five models utilized in the study

Model No.	Range of variables								
	<i>d</i> (cm)	<i>b</i> (cm)	θ	<i>y</i> (cm)	<i>B</i> (cm)	Q_t (m ³ /s)	<i>h</i> / <i>y</i>	<i>h</i> / <i>b</i>	<i>h</i> / <i>d</i>
1	0	0	60	28	25	0.0015–0.0135	0.21–0.68	–	–
2	1.25	5	60	26.75	25	0.0015–0.0091	0.18–0.57	0.96–3	3.84–12.16
3	2.5	5	60	25.5	25	0.0028–0.012	0.26–0.7	1.36–3.56	2.72–7.12
4	3.75	5	60	24.25	25	0.006–0.0135	0.4–0.75	1.96–3.62	2.6–4.8
5	5	5	60	23	25	0.008–0.0135	0.46–0.75	2.12–3.46	2.12–3.46

For this purpose, it was inferred that the discharge through a combined structure depends upon geometric, kinematic, and dynamic variables:

$$\{Q_t, g, h, \mu, \theta, \sigma, \rho, v, d, b, y, B\} \tag{5}$$

where Q_t is total discharge through the structure, g is gravitational acceleration, h is water head over the weir, μ is fluid dynamic viscosity, θ is the top angle of the triangular weir, σ is surface tension, ρ is flow density, v is fluid velocity, d is gate height, b is gate width, y is the distance between top of the gate and bottom of the weir, and B is channel width (all shown in Fig. 2). With a total of twelve independent parameters and three major quantities (length, mass, and time), nine dimensionless variables were derived based on Buckingham π theorem:

$$\frac{Q_t}{b\sqrt{0.125g}(H-d)^{1.5}} = f\left(\text{Re}, \text{We}, \text{Fr}, \theta, \frac{h}{d}, \frac{h}{y}, \frac{h}{b}, \frac{h}{B}\right) \tag{6}$$

where Re, We, and Fr are Reynolds, Weber, and Froude numbers, respectively. In this study, water depth over the weir–gate was sufficiently high and surface tension (and Weber number) effects were neglected. Furthermore, the effect of viscosity (Reynolds number) was neglected due to dominance of a turbulent flow and relatively high discharges through the models. The term $\frac{Q_t}{b\sqrt{0.125g}(H-d)^{1.5}}$ on Eq. 6 was considered as a representative for Froude number (F_r), and the number itself on the right-hand side of the

equation was removed. θ was constant in all models, and therefore, it was concluded that the term $\frac{Q_t}{b\sqrt{0.125g}(H-d)^{1.5}}$ (a dimensionless discharge, or discharge coefficient C_d) is a function of three dimensionless ratios only:

$$C_d = \frac{Q_t}{b\sqrt{0.125g}(H-d)^{1.5}} = f\left(\frac{h}{d}, \frac{h}{b}, \frac{h}{y}\right) \tag{7}$$

The conventional discharge equation for a triangular weir is a function of $h^{2.5}$ and for a rectangular gate a function of $H^{0.5}$ (Munson et al. 1994). Therefore, one may expect discharge through a combined triangular weir–rectangular gate structure (Q_t) to be a function of a water head indicator somewhere between h and H , to a power between 0.5 and 2.5. Hence, for the combined structure authors proposed Eq. 7, where discharge is considered a function of $(H-d)^{1.5}$.

2.2 Soft Computing Models

MLP and SVR soft computing models were constructed with three non dimensional parameters ($\frac{h}{d}, \frac{h}{b}, \frac{h}{y}$) as their inputs and the discharge coefficient as their output parameter. 70% of the data set was randomly selected from different experimental models and used to train the models, while the remaining 30% of the data set was used for models validation.

2.2.1 Multilayer Perceptron (MLP) Model

ANNs are based on the present understanding of biological nervous system, though much of the biological detail is neglected (Ozkan and Kaya 2010). They are generally used to predict an output vector based on known values in the input vector, especially where the relationships between the two are complex or nonlinear (Malekmohamadi et al. 2011). A typical configuration for an MLP model, a special class of ANNs, is shown in Fig. 3, where a set of data ($x_1; x_2; \dots$) is first fed into the network through the input layer. The data pass through one or more hidden layers and are finally outputted as predicted output, y (Bateni et al. 2007). The number of hidden layers determines complexity of the network, as a greater number of hidden layers increase the number of connections in the ANN.

In an MLP, neurons receive inputs from their upstream interconnections and generate outputs by their transformation with an appropriate nonlinear transfer function (Lee et al. 2007). In the case of sigmoid transfer function, for instance, the output y_j from j th neuron in the layer is determined by:

$$y_j = f\left(\sum w_{ij}x_i\right) = \frac{1}{1 + e^{-\left(\sum w_{ij}x_i\right)}} \quad (8)$$

where w_{ij} is the weight of the connection joining j th neuron in the layer with i th neuron in the previous layer and x_i is the value of i th neuron in the previous layer.

In an ANN training process, input and known output data are provided to the model simultaneously, and inter-connection weights are adjusted to minimize the output error. Once the model is successfully trained, it is tested with a validation data set whereby the accuracy of model's prediction is evaluated by comparing the model output with observed values.

In this study, a three-layer feed-forward back-propagation network with seven neurons in the hidden layer was used as the MLP model. Optimum number of neurons in the hidden layer (7 neurons) was determined through a trial and error process. Therefore, the final architecture of MLP

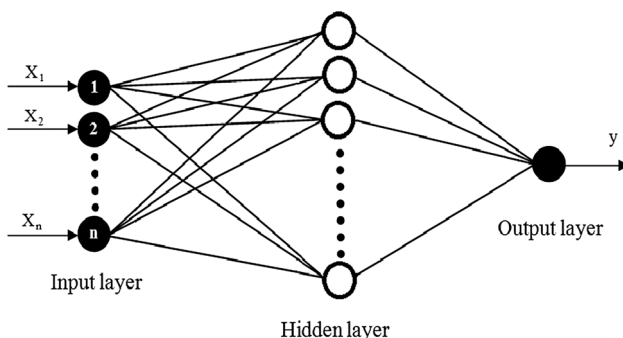


Fig. 3 A typical three-layer MLP neural network model

configuration in this study was 3-7-1 (Homayoon et al. 2010; Keshavarzi et al. 2012). A hyperbolic tangent sigmoid function and a linear function were used as transfer functions in the second and the third layers, respectively, and Levenberg–Marquardt optimization method was used for the network training.

2.2.2 Support Vector Regression (SVR) Model

Vapnik (1995) introduced support vector machines (SVM) as a type of supervised machine learning technique belonging to a family of generalized linear classifiers. SVM is based on structural risk minimization (SRM) concept, as opposed to empirical risk minimization (ERM) approach, commonly employed within statistical learning methods. SRM minimizes an upper bound on the generalization error, as opposed to ERM which minimizes training data error. It is this difference that equips SVM with a greater potential to generalize. In addition, solutions offered by traditional ANN may tend to fall into a local optimal solution, whereas a global optimum solution is guaranteed in an SVM. SVM may be applied to both classification and regression problems (Jahangirzadeh et al. 2014). For further details on SVM methods, authors suggest Vapnik (1998) and Kecman (2001).

SVR finds a function that has at most a limited deviation from the actual target output vector for a given training data and has to be as flat as possible (Pal et al. 2011). SVR models depend on a kernel function and user defined parameters such as kernel specific parameter (γ), size of error insensitive zone (ε), and regularization cost parameter (C) which control model's tolerance to error. Application of any SVR model involves optimization of cost parameter (C), kernel type, and kernel specific parameter (γ).

In nonlinear SVR, a kernel function simplifies the learning process by changing the representation of data in the input space to a linear representation in a higher-dimensional space, i.e., feature space (Hong et al. 2012). Several choices exist for a kernel function k , including linear, polynomial, and Gaussian radial basis functions. Gaussian function used in the current study is defined as (Hong et al. 2012):

$$k(x_i, x) = \exp\left\{-\gamma|x - x_i|^2\right\} \quad (9)$$

which is most commonly used to map samples into a higher-dimensional space to better handle nonlinear problems (Goyal and Ojha 2011). A large number of trials were carried out and statistical indices (highest correlation coefficient, smallest mean absolute error, MAE, and root mean-squared error, RMSE) were employed to find the optimum combination values for C and γ . In this study, $\gamma = 1$, $C = 5$, and $\varepsilon = 0.1$ were found to provide the best

results. For further details on SVR, readers may refer to Vapnik (1995).

3 Results and Discussion

Effects of each dimensionless ratio in Eq. 7 on the total discharge and its coefficient were studied in four combined weir–gate and a weir-only ($d = 0$ mm) structures. Figure 4 depicts measured heads and discharges for all physical models. As expected, total discharge (Q_t) increased with increasing head (h), however, at the same discharge, with increasing gate opening (d), water head over the weir decreased. In other words, as the gate opening increased, more discharge passed through it and less over the weir, causing a decrease in water elevation. The decrease in water head over the weir was greater at low discharges ($Q_t \leq 0.01$ m³/s). For instance, it decreased 23.4% from 0.128 m (for $d = 0$ mm) to 0.098 m (for $d = 37.5$ mm) at 0.0053 m³/s, but decreased 5.2% from 0.191 m (for $d = 0$ mm) to 0.181 m (for $d = 37.5$ mm) at 0.0135 m³/s.

At low discharges, the gate (and its opening) may be considered as the main water head controller compared to the weir, while weir would mainly control water level at high discharges ($Q_t > 0.01$ m³/s).

As expected, discharge and its coefficient were directly proportional for all gate openings (Fig. 5). At the same discharge, however, discharge coefficient increased with increasing gate opening (d). For instance, at $Q_t = 0.008$ m³/s, C_d increased from 0.55, to 0.59, 0.62 and 0.74 when d increased from 12.5, to 25, 37.5, and 50 mm, respectively (Fig. 5).

Figure 6 depicts observed discharges for weir-only against the theoretical equation ($Q_t = \frac{8}{15} C_d \tan \frac{\theta}{2} \sqrt{2gh}^{2.5}$) for a triangular sharp-crested weir (Bos 1989). As shown, observed data agree very well with the theoretical discharges ($R^2 = 0.992$), suggesting an overall data reliability.

Figure 7 shows variations of discharge coefficient (C_d) against h/d for different gate openings (d). In general, C_d consistently increased with increasing h/d for all gate openings. However, this increase was sharp at high d 's and gentle at low ones. For instance, the slope of trend lines for

Fig. 4 Variation of discharge versus h for all physical models

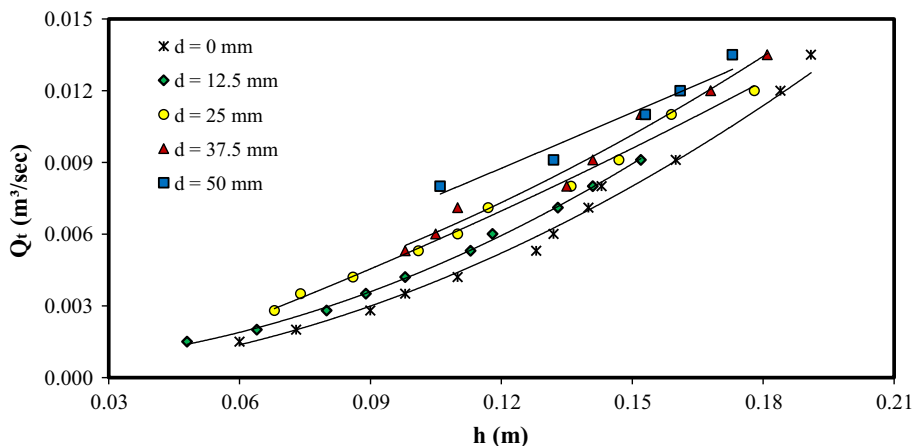
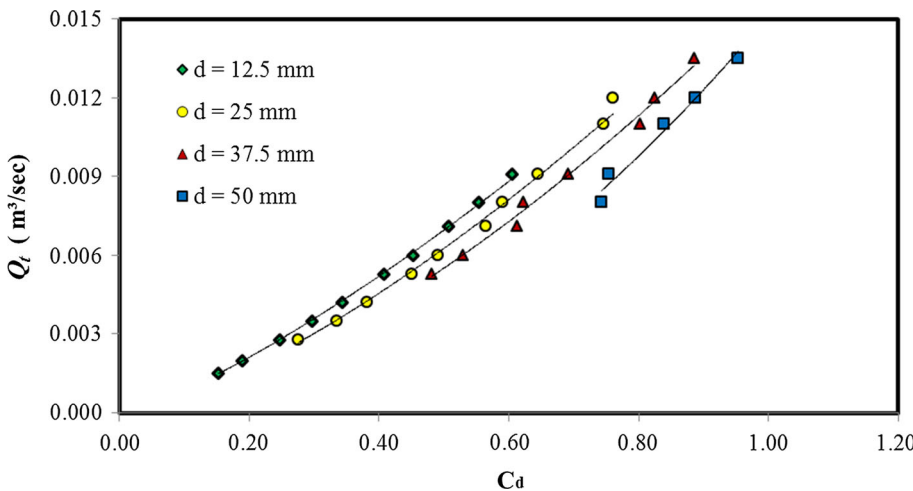


Fig. 5 Variation of discharge versus its coefficient for all combined models



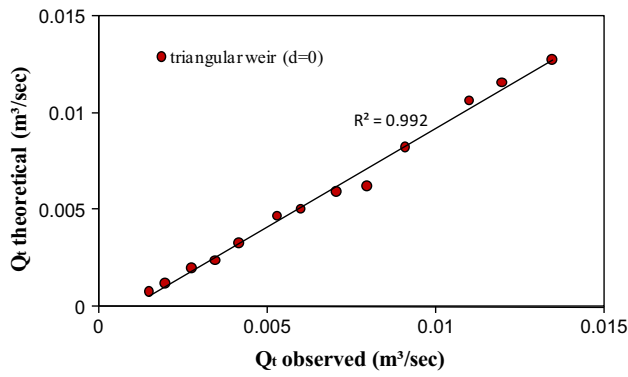


Fig. 6 Comparison between observed and theoretical discharges

$d = 12.5$ mm and $d = 50$ mm is 0.057 and 0.158, respectively. One may conclude that careful considerations should be given to water head measurements and C_d calculations, especially at high d values.

Fig. 7 Variation of discharge coefficient (C_d) for combined weir–gate structure versus h/d for different gate openings

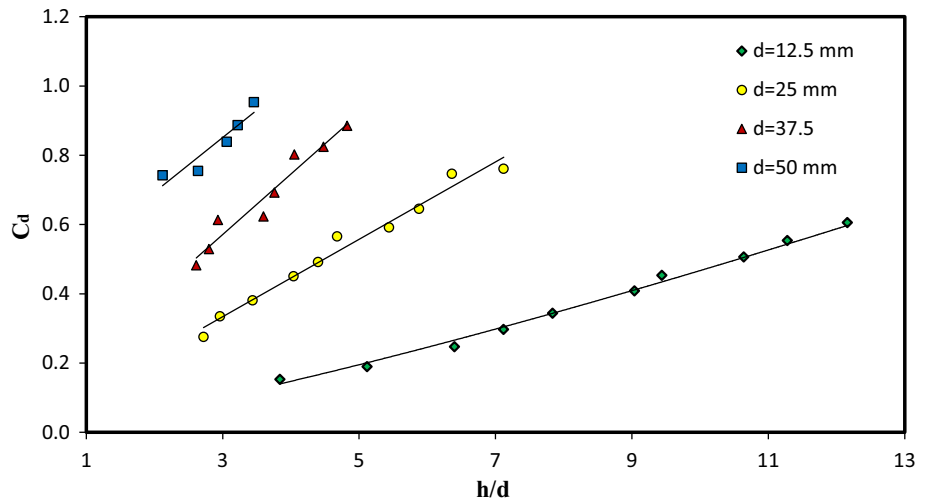
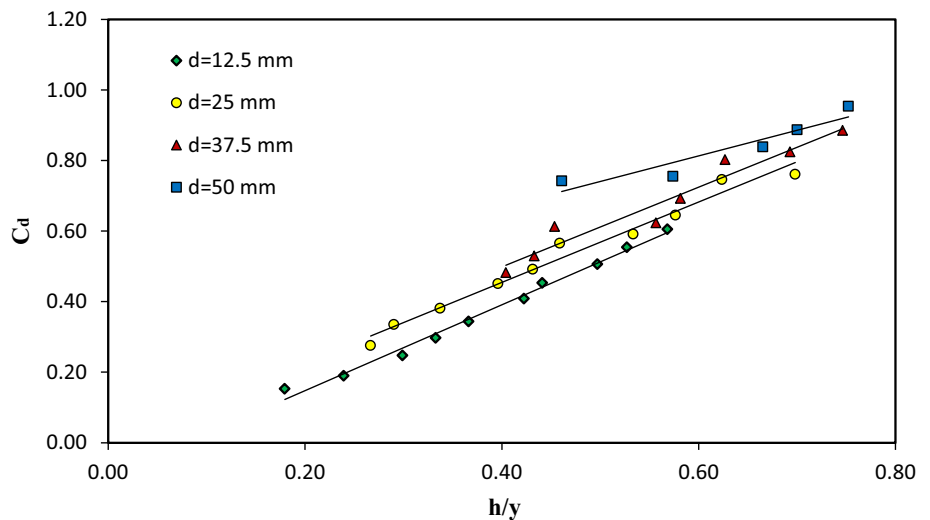


Fig. 8 Variation of discharge coefficient (C_d) for combined weir–gate structure versus h/y for different gate openings



Figures 8 and 9 show variations of discharge coefficient (C_d) for combined weir–gate structures versus h/y and h/b , respectively. In both figures, with constant d , as h/y or h/b increases, discharge coefficient increases. Any constant d (and the corresponding trend line) in these figures refers to a certain physical model, where not only d , but also b and y are constants, implying that the trend line reflects C_d variation as a function of h . As h is proportional to Q_t , it may be concluded that total discharge is directly proportional to discharge coefficient (C_d) in any combined weir–gate structure.

3.1 Discharge Coefficient Prediction

In this study, capacity of MLP and SVR models to determine complex relationships was utilized to predict the discharge coefficient of a combined weir–gate structure. Figure 10 shows predicted versus observed coefficients for

Fig. 9 Variation of discharge coefficient (C_d) for combined weir-gate structure versus h/b for different gate openings

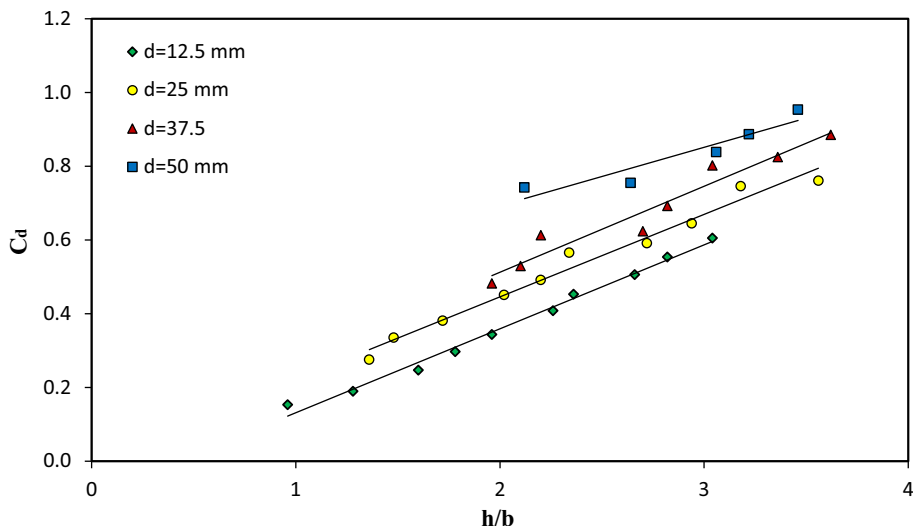
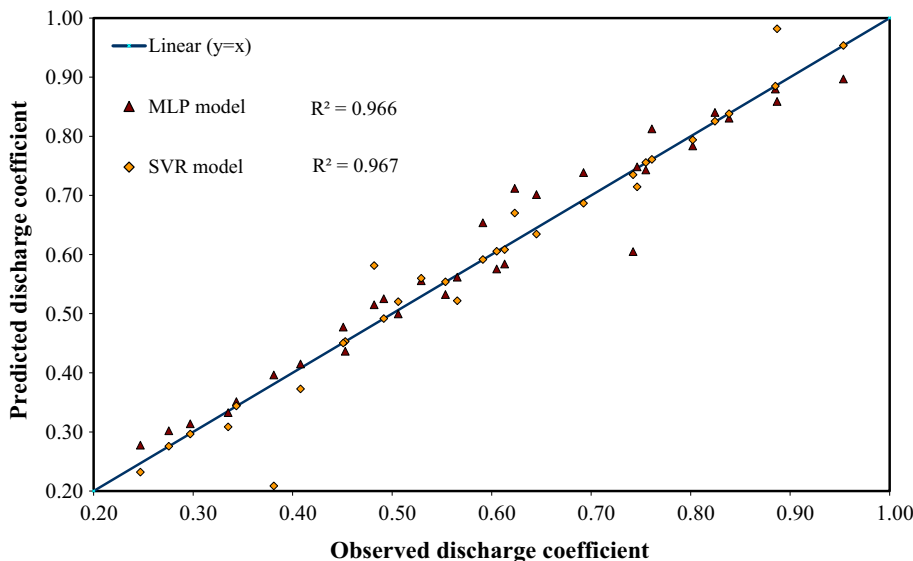


Fig. 10 Predicted versus observed discharge coefficients (C_d 's) for MLP and SVR models



both MLP and SVR models. As shown, both models predict C_d more accurately when it is smaller ($0.2 < C_d < 0.5$) compared to larger ($0.5 \leq C_d < 1$). However, R^2 values of 0.966 and 0.967 for MLP and SVR models, respectively, show a very good agreement between predicted and observed C_d 's over the entire range. Ranges of errors for MLP and SVR models are $(-0.088$ to $0.138)$ and $(-0.099$ to $0.172)$, respectively.

Figure 11 shows experimental data along with MLP and SVR results for training and validating data sets. As shown, data numbers 1–23 belong to the training, and 24–33 belong to validating data sets. In general, both models predict discharge coefficients well; however, MLP appears to demonstrate a better performance over SVR in the validation data set. A comprehensive accuracy analysis would evaluate performance of each model, quantitatively.

Root mean-squared error (RMSE), mean absolute error (MAE), and R^2 criteria were used to evaluate MLP and SVR model results more accurately. RMSE indicates the goodness of fit related to high-discharge coefficient values, whereas MAE measures a more balanced perspective of the goodness of fit at moderate discharge coefficients. They are defined as:

$$RMSE = \sqrt{\frac{1}{N} \sum_{i=1}^N (Y_i \text{ observed} - Y_i \text{ estimated})^2} \tag{10}$$

$$MAE = \frac{1}{N} \sum_{i=1}^N |Y_i \text{ observed} - Y_i \text{ estimated}| \tag{11}$$

where N is the number of data, and Y_i is the discharge coefficient, in this study. RMSE, MAE, and R^2 values for MLP and SVR models are shown in Table 2.

Fig. 11 Comparison of observed data with MLP and SVR model results during training and validation

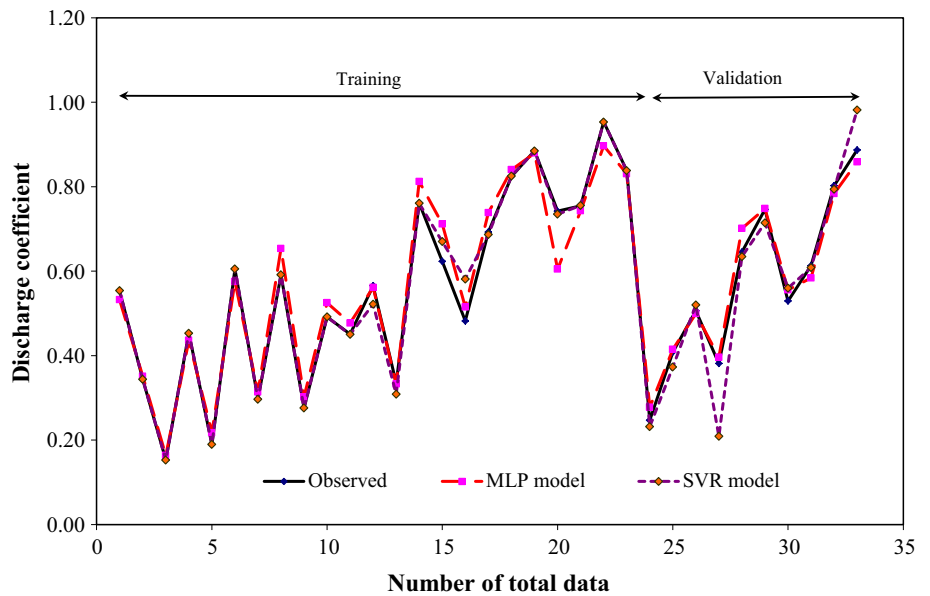


Table 2 Statistical indices for C_d 's estimated by MLP and SVR models

Soft computing model	Data set	Statistical indices		
		RMSE	MAE	R^2
MLP	Training data	0.045	0.032	0.961
	Validation data	0.027	0.022	0.984
	Total data	0.04	0.029	0.966
SVR	Training data	0.025	0.01	0.98
	Validation data	0.065	0.042	0.948
	Total data	0.042	0.02	0.967

As shown, RMSE, MAE, and R^2 values are better for SVR model compared to MLP, in training data. However, for validation data set, these statistical indices are better for

MLP model compared to SVR. For the total data set, on the other hand, the indices are very close in both models. Considering the fact that accuracy of validation data set is more important than training data set, it is concluded that MLP model may be used as an accurate and efficient model to predict discharge coefficient for a combined triangular weir–rectangular gate structure.

3.2 Comparing the Results with Existing Equations

As explained earlier, there are four main regression equations in the literature that predict discharge in a combined structure of triangular weir–rectangular gate (Eqs. 1: El-Saiad et al. 1995; 2: Negm et al. 1997; 3: Alhamid et al. 1997; and 4: Hayawi et al. 2008). It should be noted that

Fig. 12 Comparison of observed data with existing equations

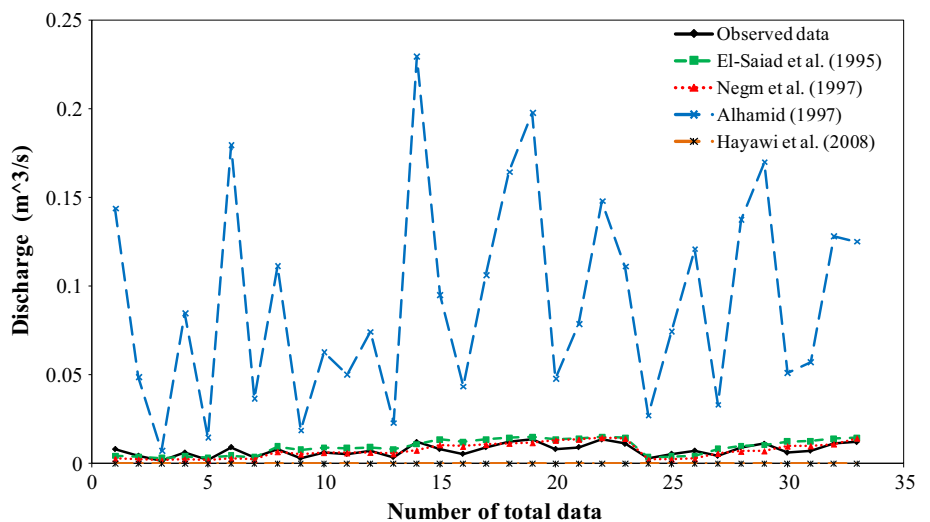


Fig. 13 Comparison of observed data, the equations, and MLP

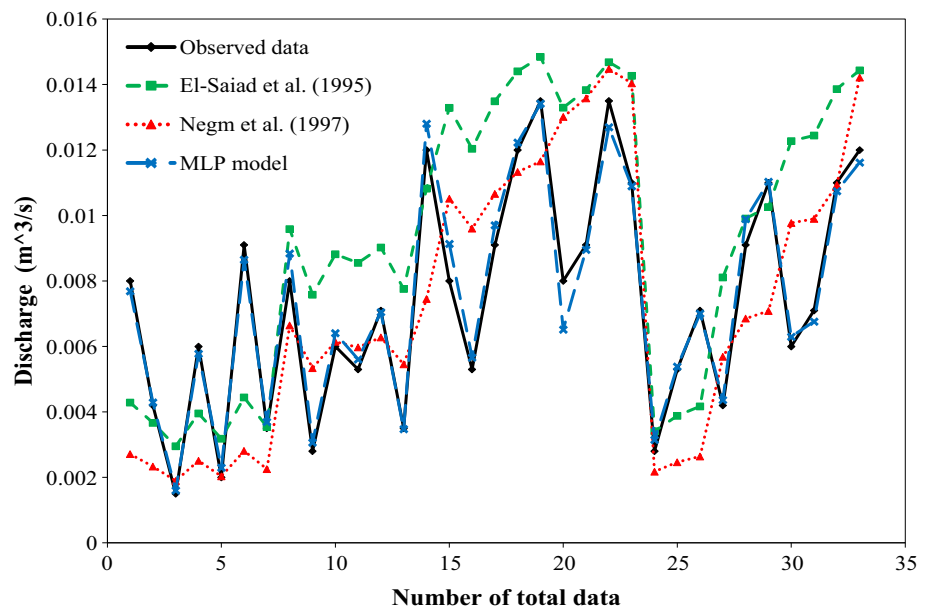


Table 3 Values of accuracy criteria for Q_t estimated by MLP and existing regression equations

Study	MAE	RMSE	R^2
El-Saiad et al. (1995)	0.0087	0.0034	0.54
Negm et al. (1997)	0.0024	0.0029	0.51
Alhamid et al. (1997)	0.083	0.099	0.77
Present study (MLP)	0.0066	7.5×10^{-20}	0.999

the range of discharge (m^3/s) for El-Saiad et al. (1995), Negm et al. (1997), Alhamid et al. (1997), and Hayawi et al.'s (2008) studies is (0.003, 0.015), (0.0019, 0.015), (0.007, 0.23), (0.000023, 0.000054) and (0.0015, 0.0135), respectively. A comparison of these equations with observed data in this study would be insightful (Fig. 12). As shown, El-Saiad et al. (1995) and Negm et al. (1997) equations match the observed data much better than Alhamid et al. (1997) and Hayawi et al.'s (2008) results, which are noticeably different. It was concluded that assuming the general form of a gate equation in Alhamid et al. (1997) and a weir equation in Hayawi et al. (2008) for the combined weir–gate structure shall be reconsidered before utilization.

Figure 13 depicts the performance of MLP model in comparison to El-Saiad et al. (1995) and Negm et al.'s (1997) equations. As shown, MLP model predicts discharges much more accurately compared to both equations. Apparently, it was due to MLP being capable of determining complex relationships more flexibly than rigid regression equations. Additionally, small differences in scales and ranges of hydraulic parameters used in each study may have caused some differences, too.

Table 3 shows RMSE, MAE, and R^2 values for MLP model and Eqs. 1, 2, and 3. Considering these statistical indices, it was concluded that MLP model predicts total discharge (Q_t) more accurately, followed by Negm et al. (1997), El-Saiad et al. (1995), and Alhamid et al. (1997) equations, respectively.

4 Conclusions

In this study, experiments with extended measuring ranges for relevant parameters were conducted on combined triangular weir and rectangular gate structures under free flow conditions to estimate discharge coefficients (C_d) and compare them with those reported in the literature. Investigating effects of three dimensionless parameters (h/d , h/b , and h/y) on C_d showed that as the parameters increase, so does discharge (Q_t) and its coefficient. At the same discharge, however, discharge coefficient increased with increasing gate opening (d). For instance, at $Q_t = 0.008 m^3/s$, C_d increased from 0.55, to 0.59, 0.62, and 0.74 when d increased from 12.5, to 25, 37.5, and 50 mm, respectively. Moreover, it was concluded that, at low discharges ($Q_t \leq 0.1 m^3/s$), the gate and its opening are the main water head controllers, while water levels at high discharges ($Q_t > 0.1 m^3/s$) are mainly controlled by the weir.

Utilized soft computing models (MLP and SVR), both predicted C_d accurately (with R^2 of 0.966 and 0.967, respectively). However, MLP was considered superior, due to better statistical indices of RMSE, MAE, and R^2 (0.027, 0.022, and 0.984, respectively) in the validation data set compared to SVR (0.065, 0.042, and 0.948, respectively).

Comparing results with existing equations showed that El-Saiad et al. (1995) and Negm et al.'s (1997) equations match the observed data much better than noticeably different Alhamid et al. (1997) and Hayawi et al.'s (2008) results. It was concluded that assuming the general form of a gate equation in Alhamid et al. (1997) and a weir equation in Hayawi et al. (2008) for the combined weir–gate structure shall be reconsidered before utilization in particular applications.

Acknowledgements Authors would like to thank Mr. Mehdi Zini-vand, Professor Mahmood Shafai-Bajestan, and Dr. Mohammad-Reza Nikoo for their invaluable help, ideas, and comments.

References

- Alhamid AA, Negm AM, Al-Brahim AM (1997) Discharge equation for proposed self-cleaning device. *J King Saud Univ* 9(1):13–24
- Altan-Sakaraya A, Kokpınar MA (2013) Computation of discharge for simultaneous flow over weirs and below gates (H-weirs). *J Flow Meas Instrum* 29:32–38
- Aydin I, Ger AM, Hincal O (2002) Measurement of small discharges in open channels by slit weir. *J Hydraul Eng ASCE* 128(2):234–237
- Aydin I, Altan-Sakarya AB, Sisman C (2011) Discharge formula for rectangular sharp-crested weirs. *J Flow Meas Instrum* 22:144–151
- Balouchi B, Nikoo MR, Adamowski J (2015) Development of expert systems for the prediction of scour depth under live-bed conditions at river confluences: application of different types of ANNs and the M5P model tree. *J Appl Soft Comput Elsevier* 34:51–59
- Bateni SM, Borghei SM, Jeng DS (2007) Neural network and neuro-fuzzy assessments for scour depth around bridge piers. *J Artif Intell Elsevier* 20:401–414
- Bautista-Capetillo C, Robles O, JÚnez-Ferreira H, Playán E (2014) Discharge coefficient analysis for triangular sharp-crested weirs using low-speed photographic technique. *J Irrig Drain Eng* 140(3):06013005
- Baylar A, Hanbay D, Batan M (2009) Application of least square support vector machines in the prediction of aeration performance of plunging overfall jets from weirs. *J Expert Syst Appl Elsevier* 36:8368–8374
- Belaud G, Cassan L, Baume J (2012) Contraction and correction coefficients for energy-momentum balance under sluice gates. In: *World environmental and water resources congress 2012*, pp 2116–2127. <https://doi.org/10.1061/9780784412312.212>
- Bilhan O, Emiroglu ME, Kisi O (2011) Use of artificial neural networks for prediction of discharge coefficient of triangular labyrinth side weir in curved channels. *Adv Eng Softw* 42:208–214
- Bos MG (1989) *Discharge measurement structures*, 3rd edn. International Institute for Land Reclamation and Improvement, Wageningen
- Chanson H, Wang H (2013) Unsteady discharge calibration of a large V-notch weir. *J Flow Meas Instrum* 29:19–24
- El-Saiad AA, Negm AM, Waheed El-Din U (1995) Simultaneous flow over weirs and below gates. *Civ Eng Res Mag* 17(7):62–71
- Emiroglu ME, Bilhan O, Kisi O (2011) Neural networks for estimation of discharge capacity of triangular labyrinth side-weir located on a straight channel. *Expert Syst Appl* 38:867–874
- French RH (1986) *Open-channel hydraulics*. McGraw Hill Book Company, New York
- Goyal MK, Ojha CSP (2011) Estimation of scour downstream of a ski-jump bucket using support vector and M5 model tree. *Water Resour Manag* 25:2177–2195
- Habibzadeh A, Vatankhah A, Rajaratnam N (2011) Role of energy loss on discharge characteristics of sluice gates. *J Hydraul Eng* 137(9):1079–1084
- Haghiabi AH, Azamathulla HM, Parsaie A (2017) Prediction of head loss on cascade weir using ANN and SVM. *ISH J Hydraul Eng* 23(1):102–110
- Hayawi HAA, Yahia AAA, Hayawi GAA (2008) Free combined flow over a triangular weir and under rectangular gate. *Damascus Univ J* 24(1):9–22
- Homayoon SR, Keshavarzi A, Gazni R (2010) Application of artificial neural network, Kriging, and inverse distance weighting models for estimation of scour depth around bridge pier with bed sill. *J Softw Eng Appl* 3:944–964
- Hong J, Goyal MK, Chiew Y, Chua LHC (2012) Predicting time-dependent pier scour depth with support vector regression. *J Hydrol* 468–469:241–248. <https://doi.org/10.1016/j.jhydrol.2012.08.038>
- Jahangirzadeh A, Shamshirband S, Aghabozorgi S, Akib S, Basser H, Anuar NB, Kiah MLM (2014) A cooperative expert based support vector regression (Co-ESVR) system to determine collar dimensions around bridge pier. *Neurocomput J* 140:172–184
- Johnson MC (2000) Discharge coefficient analysis for flat-topped and sharp-crested weirs. *J Irrig Sci* 19(3):133–137
- Juma IA, Hussein HH, Al-Sarraj MF (2014) Analysis of hydraulic characteristics for hollow semi-circular weirs using artificial neural networks. *Flow Meas Instrum* 38:49–53
- Kecman V (2001) *Learning and soft computing: support vector machines, neural networks and fuzzy logic models*. MIT Press, Cambridge
- Keshavarzi A, Gazni R, Homayoon SR (2012) Prediction of scouring around an arch-shaped bed sill using Neuro-Fuzzy model. *Appl Soft Comput* 12:486–493
- Khalili Shayan H, Farhoudi J (2013) Effective parameters for calculating discharge coefficient of sluice gates. *Flow Meas Instrum* 33:96–105
- Lee TL, Jeng DS, Zhang GH, Hong JH (2007) Neural network modeling for estimation of scour depth around bridge piers. *J of hydrodynamic* 19(3):378–386
- Lozano D, Mateos L, Merkle G, Clemmens A (2009) Field calibration of submerged sluice gates in irrigation canals. *J Irrig Drain Eng* 135(6):763–772
- Malekmohamadi I, Bazargan-Lari MR, Kerachian R, Nikoo MR, Fallahnia M (2011) Evaluating the efficacy of SVMs, BNs, ANNs and ANFIS in wave height prediction. *J Ocean Eng* 38:487–497
- Martínez J, Reca J, Morillas MT, López JG (2005) Design and calibration of a compound sharp-crested weir. *J Hydraul Eng* 131(2):112–116
- Mohammadpour R, Shaharuddin S, Chang CK, Zakaria NA, Ab Ghani A, Ngai WC (2015) Prediction of water quality index in constructed wetlands using support vector machine. *Environ Sci Pollut Res* 22(8):6208–6219
- Munson BR, Young DF, Okiishi TH (1994) *Fundamentals of fluid mechanics*, 2nd edn. Wiley, New York
- Negm AM (1995) Characteristics of combined flow over weirs and under gate with unequal contractions. In: *Proceedings of 2nd international conference on hydro-science and engineering, China*, vol 2(A), pp 285–292
- Negm AM (2000) Characteristics of simultaneous overflow—submerged underflow: (unequal contractions). *Eng Bull* 35(1):137–154
- Negm AM, El-Saiad AA, Saleh OK (1997) Characteristics of combined flow over weirs and below submerged gates. In:

- Proceedings of Al-Mansoura engineering 2nd international conference on (MEIC'97) Al-Mansoura, Egypt, vol 3(B), pp 259–272
- Negm AM, Albarahim AM, Alhamid AA (2002) Combined free flow over weirs and gate. *J Hydraul Res* 40(3):359–365
- Ozkan F, Kaya T (2010) Using intelligent methods to predict air-demand ratio in venturi weirs. *J Adv Eng Softw* 41:1073–1079
- Pal M, Singh NK, Tiwari NK (2011) Support vector regression based modeling of pier scour using field data. *Eng Appl Artif Intell* 24(5):911–916
- Parsaie A, Haghiabi AH, Saneie M, Torabi H (2017) Predication of discharge coefficient of cylindrical weir-gate using adaptive neuro fuzzy inference systems (ANFIS). *Front Struct Civ Eng* 11(1):111–122
- Qu J, Ramamurthy AS, Tadayon R, Chen Z (2009) Numerical simulation of sharp-crested weir flows. *Can J Civ Eng* 36(9):1530–1534
- Rajaratnam N (1977) Free flow immediately below sluice gates. *Proc J Hydraul Div ASCE* 103(HY4):345–351
- Swamee PK (1988) Generalized rectangular weirs equations. *Proc J Hydraul Eng ASCE* 114(8):945–949
- Swamee PK (1992) Sluice gate discharge equations. *Proc J Irrig Drain Eng, ASCE* 118(1):57–60
- Vapnik VN (1995) *The nature of statistical learning theory*. Springer, New York
- Vapnik VN (1998) *Statistical learning theory*. Wiley, New York